5-10-2020

NF-κB Subunits p50 and RelA Contribute to Oncogenesis in a Mouse Model of ST-EPN

Ericka J. Randazzo

University of Connecticut - Storrs, ericka.randazzo@uconn.edu

NF-κB Subunits p50 and RelA Contribute to Oncogenesis in a Mouse Model of ST-EPN

Ericka Jade Randazzo

B.S., Physiology and Neurobiology, University of Connecticut, 2019

B.S., Pathobiology, University of Connecticut, 2019

A Thesis

Submitted in the Partial Fulfillment of the

Requirements for the Degree of

Master of Science

At the

University of Connecticut

2020

2020

APPROVAL PAGE

Masters of Science Thesis

NF-κB Subunits p50 and RelA Contribute to Oncogenesis in a Mouse Model of ST-EPN

Presented by

Ericka Jade Randazzo, B.S.

Major Advisor _____

Joseph LoTurco, PhD

Associate Advisor _____

Jianjun Sun, PhD

Associate Advisor _____

Akiko Nishiyama, PhD

University of Connecticut

2020

AKNOWLEDGEMENTS

First and foremost, I would like to thank my major thesis advisor, Dr. Joseph LoTurco. Upon entering the lab, Dr. LoTurco personally taught me basic lab techniques and principles. His door was always open for any questions I had regarding data interpretation, lab techniques, presentations, courses, and so forth. His mentorship has shaped me into the scientist I am today and has guided me in my career pursuits. Words cannot express my gratitude for his time, enthusiasm, guidance, and kindness.

I would also like to thank everyone in the LoTurco Lab. In particular, I would like to thank Jesse Dunnack, for "showing me the ropes" and completing much of the foundational work that enabled completion of this project. I would like to thank the current lab technician, Kevin Truong, for assisting me in much of the data collection of this project. Completion of my thesis would not have been possible without his efforts, support, and friendship. I am also grateful for Alix Battison, Justin Fang, James He, and Gülcan Akgül in the lab, for their experimental expertise, advice, and comradery during my time in the lab.

I am deeply grateful for the contributions from my collaborators. In particular, I would like to thank Dr. Jianguo Wu, for his work in performing the immunoprecipitation analysis for this project. I would like to thank Christopher O'Connell, the Director of the Advanced Light Microscopy Facility at UConn, for his guidance and assistance in utilizing the microscopes and performing the colocalization and tumor area analyses used in this study. I would also like to thank my committee members, Dr. Nishiyama and Dr. Sun, for their guidance and support through my thesis. I am also deeply grateful for all of the Vivarium staff – especially Richard Simoniello, Teresa Samuels, and Briana Lechkun - for maintaining and caring for the animals used in these experiments.

I would also like to acknowledge my supplemental grant sponsored by the Arnold and Mable Beckman Foundation. This program helped me connect with scientists across the country and verified my passion for science, fueling my future career interests. The program also provided funding that made much of the foundational work needed for the completion of this project possible.

I am also deeply grateful for the entire Physiology and Neurobiology Department. They have created a positive environment in which to develop and learn over the last five years – providing resources, support, and stimulating curiosity. I would like to thank my teammates and coaches for supporting my enthusiasm for science and supporting me in presentations and conferences. Last but not least, I would like to thank my parents for their amazing support throughout my academic journey. Regardless of my academic pursuits, they have continued to support me in any and every way they can.

TABLE OF CONTENTS

LIST OF FIGURES

ABSTRACT

The NF-κB pathway has been demonstrated to be upregulated in supratentorial ependymoma (ST-EPN). Whether the different NF-κB transcription factors contribute to ST-EPN tumorigenesis however, has not been investigated. We assessed the degree to which NF-κB subunits p50 and RelA interact with the ST-EPN fusion mutation C11orf95-RELA in regulating gene expression via colocalization analysis in Hek293T cell nuclei. We analyzed the functional outcomes of overexpression of p50 or RelA, or CRISPR/Cas9-mediated knockdown of p50, in combination with the C11orf95-RELA fusion i*n vivo* by examination of tumor area in P14 – 21 CD1 mice. We further analyzed the effects each of these conditions have on transformed cell morphology using immunohistochemistry and microscopy. Our results show that the C11orf95-RELA fusion and RelA more significantly colocalize with the C11orf95-RELA fusion than does p50 in Hek293T cell nuclei. Overexpression of RelA in combination with the C11orf95-RELA fusion generates larger tumors by P21, while CRISPR knockdown of p50 in neural progenitor cells reduces tumor size, in comparison to age matched controls. While overexpression of RelA with the WT C11orf95-RELA fusion generates tumors that recapitulate WT tumor morphology, overexpression of p50 generates tumors with significantly altered transformed cell morphology. Our data demonstrates that both NF-κB subunits RelA and p50 are capable of interacting with the oncogenic C11orf95-RELA fusion, and that such interaction may contribute to ST-EPN tumorigenesis.

INTRODUCTION

Categorization of Ependymoma

Brain tumors are the most common childhood solid malignancy, and because of remarkable advances in treating many cancers outside of the brain, they have become the leading cause of cancer mortality in children. Ependymomas are a class of primary neuroepithelial tumors of the central nervous system that can arise along the entire neuroaxis including the ventricular system of the cerebral hemispheres, the hindbrain, and the spinal cord (Pajtler et. Al. 2016). The neoplasms can be further subdivided into three groups based upon their compartmental location and genetic features: posterior fossa, spinal cord, and supratentorial. These malignancies can occur in both children and adults, although the occurrence of each subtype differs based upon age group, and are overall more common in children than adults. According to the 2014 report published by the Central Brain Tumor Registry of the United States (CBTRUS), ependymomas account for approximately 10% of primary CNS tumors in children and adolescents ages 0 – 19 years, most of which arise in the posterior fossa. In contrast, ependymomas comprise about 5% of adult CNS tumors, the majority of which arise in the spinal cord and posterior fossa region (Torre et. Al. 2019). There also appears to be a racial disparity in ependymoma incidence rate, with a rate of 0.40 per 100,000 incidences in white populations versus 0.27 in African Americans (Wu, Armstrong, and Gilbert, 2016).

The WHO classification of CNS tumors is currently accepted as the standard classification system, and categorizes ependymomas as grade I, II, or III. Grade I ependymomas include slow-growing ependymomas such as subependymomas and myxopapillary ependymomas. These are often slow-growing and are typically considered benign neoplasms. On MRI scans, grade I ependymomas appear to be sharply circumscribed and demarcated nodular masses. Grade II ependymomas are designated as ependymoma. Multiple histological variants have been identified, including papillary, clear cell, cellular, and tanycytic ependymomas. Nonpalisading geographic foci of necrosis are characteristic histological features of Grade II ependymoma tumors. In contrast, Grade III tumors are designated as anaplastic

ependymomas. Pathognomonic histological features of these malignancies include perivascular pseudorosettes, which originate from tumor cells arranged radially around blood vessels with a perivascular anuclear zone, and true ependymal rosettes or tubules, which are ependymal cells arranged around a central lumen. In comparison to the nonpalisading geographic foci of necrosis in Grade II tumors, Grade III tumors present with pesudopalisading necrosis and microvascular proliferation. Hypercellularity, vigorous mitotic activity, and hyperchomatic and pleomorphic nuclei are also frequently observed in anaplastic ependymomas. Clinical manifestation of all grades are largely location dependent, but may include chronic back pain and increased intracranial pressure (Godfraind C. 2009, Wu, Armstrong, and Gilbert, 2016).

Identification of prognostic factors in ependymomas remains an important but controversial topic – in part due to the difficulty in accurately diagnosing ependymomas. In a study of 2,408 ependymoma cases from the Surveillance, Epidemiology and End Results (SEER) database between 1997 and 2005, Rodriguez et. Al. identified the following factors to be associated with poor clinical outcome: younger age, higher tumor grade, male sex, intracranial location, and failure to undergo extensive surgical resection (Rodriguez et. Al. 2009). However, with growing data demonstrating histological, molecular, and genetic differences between pediatric and adult ependymomas, prognostic factors may be different for pediatric patients than those for adults and therefore must be analyzed separately. In a 2012 study from the SEER database, Amirian et. Al. identified anaplastic histology and infratentorial tumor location to be associated with increased mortality rate in pediatric patients, while supratentorial tumor location was associated with higher mortality rate in adult patients (Amirian et. Al 2012).

To better account for variabilities in clinical feature information, sample number and study data quality from different databases, the Collaborative Ependymoma Research Network (CERN) developed a multi-institutional, clinically annotated tissue repository. This repository collected a wide variety of information from each sample in an effort to better define clinical and demographic factors associated with progression free survival (PFS) in adult ependymoma patients. Results indicated a significant

difference in PFS by tumor location. The median time to progression was only 3.9 years for the supratentorial region, 12.3 years for the infratentorial brain region, and was not reached by patients with a spinal cord location. In addition, patients younger than 44 years of age at the time of diagnosis had a significantly shorter PFS than those older than 44 years of age. These results reaffirm those found in earlier studies, and highlight a need for greater investigation of supratentorial ependymoma to reduce the 3.9 year PFS (Vera-Bolanos, Aldape, Yuan et. Al 2015). The CREN tissue repository was also utilized to correlate individual histological features with clinical outcomes and specific ependymoma tumor biology. Microvascular proliferation, elevated mitotic rates, and extensive ependymal canal formation were found to be associated with a worse progression free survival in supratentorial tumors in comparison to posterior fossa or spinal ependymomas. These histological features may serve as better measures of prognostic importance than WHO grade in assessment of ependymoma subtypes, and suggest that the clinical relevance of specific histological features in ependymomas appears to be related to the anatomical sites of their origins.

In spite of these efforts to create histological criteria for categorizing ependymoma into risk groups, extensive variability is seen in outcomes despite similarities in microscopic characteristics (Mangalore et. Al. 2015). This suggests that ependymomas have discrete tumor biology that cannot be fully explained by traditional histological classification. As a result, several molecular analyses have been undertaken to try to elucidate the pathogenesis of ependymoma tumors in an effort to create better prognostic groupings and potentially new therapeutic targets (Yao, Mack, and Taylor 2011; Pietsch et. Al. 2014; Parker et. Al. 2014; Wu, Albertson, and Gilbert 2016). The following will review the molecular genetic basis of ependymoma – including familial genetic risk factors, early cytogenetic detections of chromosomal abnormalities, and the identification of candidate driver events and pathways in ependymoma tumorigenesis.

Genetic Basis of Ependmoma

Like other cancers, ependymoma is a genetic disease. However, unlike many other cancers for which existing familial cancer syndromes provide important clues for understanding tumorigenic mechanisms, there are few known familial ependymoma syndromes. While there is increased incidence of spinal ependymomas in patients with a loss of neurofibromatosis type 2 (NF2) on chromosome 22q, the *NF2* gene does not appear to be the critical tumor suppressor gene on chromosome 22q that is involved in intracranial ependymoma tumorigenesis (Yao, Mack, and Taylor 2011), Ependymoma has also been reported in patients with germline mutations in the *TP53* tumor suppressor gene. However, these occurrences, as well as somatic mutations in *TP53* in ependymomas are rare, thus weakening support for the role of p53 in ependymoma tumorigenesis (von Haken MS, White EC, Daneshvar-Shyesther L, et. Al. 1996).

Over the years, cytogenetic studies using karyotyping and comparative genomic hybridization (CGH) have reported numerous broad chromosomal abnormalities in ependymoma. Several studies over the last two decades have also mounted building evidence supporting the notion that ependymomas are highly heterogeneous tumors and can be classified into distinct disease subtypes based upon anatomical tumor location, patient age, and genetic alterations. Combining such findings, cytogenetic abnormalities have been further subdivided with distinct epednymoma disease subtypes. Commonly observed genomic abnormalities in pediatric ependymomas include gains of chromosomes 1q, 5, 7, 8, 9, 11, 18, and 20, as well as loss of chromosomes 1p, 2, 3, 6/6q, 9p, 13p, 17, and 22. In adult ependymomas, chromosomes 2, 5, 7, 9, 12, 18, and X are commonly gained whereas chromosomes 6, 10, 13q, 14q, 16, and 22/22q are frequently lost (Kilday JP, Rahman R, Dyer S, et al. 2009). Location-specific genomic abnormalities are roughly similar in children and adults in regards to intracranial versus spinal ependymomas. In addition to genomic gains and losses, cytogenetic studies have also identified translocations occurring frequently within the ependymoma genome. These often involve chromosomes 1, 11, and 22 (Mack and Taylor, 2008; de Bont, Packer, and Michiels et. Al. 2008; Aschero, Vallero, Morra et. Al. 2010).

Although the identified genomic gains and losses in ependymomas support findings for profile-based stratification, they provide little insight into the tumor suppressors, oncogenes, and molecular pathways responsible for the development of ependymoma. In addition, chromosome-level aberrations are broad and typically span numerous genes, making it difficult to discriminate driver genetic events from indirect passenger events. The use of array CGH (aCGH) in fine-mapping copy number variations in cancer, in combination with analysis of gene expression levels, has expedited our understanding of potential molecular genetic aberrations that may be driving ependymoma tumorigenesis. With advances in microarray and next-generation sequencing technologies, examination of ependymoma genetics has largely shifted towards detailed analysis of copy number variations and gene expression levels.

Genetic Aberrations in Supratentorial Ependymoma

While there have been several studies analyzing molecular genetic aberrations in posterior fossa and spinal ependymomas, this review will focus on supratentorial ependymomas – the subject of this study. In 2010, Korshunov et. Al. identified homozygous deletion of the *CDKN2A* locus of chromosome 9 to be a characteristic feature of anaplastic supratentorial ependymomas, and a reliable independent indicator of unfavorable patient outcome (Korshunov et. Al. 2010). These findings supported earlier work by Taylor et. Al. that identified *CDKN2A* deletion to be characteristic of supratentorial, but not posterior fossa nor spinal ependymomas (Taylor et. Al. 2005).

In 2016, Pajtler, et. Al. assessed the DNA methylation profiles of ependymomas and suggested that the three regional classifications of ependymoma neoplasms could be further classified into nine different subgroups. Of the nine subgroups, one was characterized by a somatic gene rearrangement of *RELA* with *C11orf95* of chromosome 11. These ependymomas occurred exclusively in the supratentorial compartment and predominantly in pediatric populations. They were further demonstrated to be the most aggressive and lethal of all ependymomas, with poor clinical outcomes. Sanger sequencing of cDNA from tumor samples by Pietsch et. Al. confirmed these findings and demonstrated that the novel fusion transcript specifically consists of the N-terminal part of C11orf95 encoding 212aa of the 678aa

hypothetical protein sequence (exons 1 and 2) fusing to RelA. Only the first three amino acids of RelA are deleted in-frame; the C-terminal RelA part of the putative fusion protein was found to contain almost the full RelA sequence.

Treatment of Ependymoma

Currently, the primary treatment for ependymoma remains to be surgical resection followed by radiotherapy. Although postoperative radiotherapy may induce stabilization and, occasionally, regression of residual disease, chemotherapy is ineffective in most adult and pediatric patients (Yao et. Al. 2011, Wu, Albertson, and Gilbert 2016). As a result, surgery and irradiation remain the mainstay for treatment of ependymoma, and the tumors are incurable in up to 40% of cases. In general, the survival rate is highest for those aged 20 – 44 years and decreases with increasing age at diagnosis. Even so, the 10-year survival rate is 66% in children and adolescents aged 0 – 19 years and only 28.1% in those over the age of 75 (Wu, Albertson, and Gilbert, 2016). Seeing as no chemotherapy regimen has prolonged overall survival in children or adults with ependymoma, and survival rates remain low, development of new therapeutic options is needed to increase survival and reduce long-term sequels of current treatments. With C11orf95-RELA fusion-positive ependymomas comprising the most lethal and aggressive of all ependyomas, a greater understanding of the pathogenesis of this ependymoma subgroup is needed for therapeutic development.

Cell of Origin of Ependymoma

In the hunt for more effective treatments for ependymoma, identification of the progenitor cell type that gives rise to the neoplasms is one of the prevailing questions in the ependymoma field. Since the discovery of cancer stem cells (CSC) in 2006 (Clarke and Fuller, 2006), the idea that a single multipotent and self-renewing stem cell-like cell gives rise to all the phenotypically diverse cells of a tumor has provided cancer researchers a practical focus point for studying the developmental and molecular events of tumorigenesis (Poppleton and Gilbertson, 2007). In order to understand the search for CSC – like cells

in ependymoma, it is important to understand the processes that regulate neurogenesis and the generation of different glial and neural cell types in the CNS.

In vertebrates, neural stem cells first appear as a layer of pseudostratified epithelium that lines the neural plate and neural tube before the onset of neurogenesis. These neuroepithelial cells (NECs) are highly polarized cells – an important feature the contributes to the fate of daughter cells after mitosis. As neurogenesis begins in the early days of embryonic development (E10 in mice), NECs give rise to radial glial cells (RGCs), which retain the polarized features of NEC. These RGCs are mitotically active, multipotent progenitor cells that possess the capacity for both symmetric and asymmetric division. When RGCs divide symmetrically, they divide to generate two identical daughter cells that resemble the parent radial glial cell, thus expanding he progenitor cell pool. In contrast, when RGCs divide asymmetrically, they generate two different daughter cells: one stem cell (derived from the basal surface of the RGC), and one cell that is fated to differentiate (generated from the apical surface of the RGC). These differentiating cells ultimately give rise to the majority of neurons, oligodendrocytes, astrocytes, and ependymal cells of the brain (Spassky et. Al. 2005). Development of the cerebral cortex is both spatially and temporally controlled by RGC divisions. In mice, symmetric divisions of RGCs dominate leading up to E11. The onset of neurogenesis occurs between E11 and E13, during which RGCs begin to divide asymmetrically. After E17, gliogenesis begins and migrating cells complete differentiation into astrocytes, oligodendrocytes, ependymal cells, and other glial cell types (Dwyer et. Al. 2016).

In normal tissues, stem cell self-renewal is tightly controlled. Deregulation of RGC division may thus play a key role in the development of ependymoma. Indeed, over the last fifteen years, several studies have generated support indicating that the cellular origin of ependymoma consists of an incompletely defined population of neural stem cells, including radial glial cells (Morest and Silver, 2003; Taylor et. Al. 2005).

The Oncogenic C11orf95-RELA Fusion in Supratentorial Ependymoma

Studies of the progenitor cell type(s) that drive(s) tumorigenesis in ependymoma are largely oversimplified unless coupled with an understanding of subtype differences among ependymoma tumors. As discussed previously, supratentorial ependymomas are now known to be widely characterized by an oncogenic fusion mutation between *C11orf95* and *RELA*. Knowledge of the physiological functions of the components in this oncogenic driver fusion mutation differ widely. The physiological function of C11orf95 is unclear. C11orf95 has previously been described as a fusion partner of the gene coding the transcription factor Mk12 in benign chondroid lipomas (Flucke et. Al. 2013). Sequence analysis indicates the presence of two putative zinc finger domains, suggesting a role for C1orf95 in transcriptional regulation.

While the physiological function of C11orf95 is largely unknown, that of RELA is well characterized. *RELA* encodes RelA, a 65-kDa protein that interacts with IκB and p50 in the central signaling complex of the NF-κB pathway. In the canonical NF-κB pathway, the NF-κB dimer is sequestered in the cytosol by its inhibitor IκB (inhibitor of NF-κB) protein. Upon activation of cell surface receptors such as Toll-like receptors and TNF cytokine receptors, a series of events occur proximal to the membrane, leading to the activation of IKK (IκB kinase). Phosphorylation of IκBs via IKK results in their proteasomal degradation, thus releasing NF-κB to translocate to the nucleus and activate gene transcription of target genes (Napetschnig & Wu, 2013).

The main physiological function of NF-κB signaling is to orchestrate inflammatory responses to both infection and tissue damage. It has also been shown to control cell proliferation and apoptosis. Not surprisingly, it is frequently found to be involved in the pathogenesis of neoplasms – especially solid tumors characterized by chronic inflammation. In addition to its implications in controlling inflammation, proliferation, and apoptosis, NF-κB signaling can further contribute to tumorigenesis by controlling

vascularization via upregulation of vascular endothelial growth factor (VEGF) and its receptor (Xie et. Al. 2010).

NF-kB Signaling in Supratentorial Ependymoma

While aberrant NF-κB signaling is a well-established driver of solid tumors, and mutations in NF-κB genes such as *RELA* have been detected as genetic drivers of various malignancies (Courtois et. Al. 2006), significant genetic evidence of pathway involvement in supratentorial ependymoma (hereafter, ST-EPN) is lacking. In 2014, Pietsch et. Al. and Parker et. Al. simultaneously published findings demonstrating that ST-EPNs carrying C11orf95-RELA fusions lead to pathological activation of the NF-κB signaling pathway (Pietsch et. Al. 2014, Parker et. Al. 2014). In the latter study, RNA-seq gene expression profiling demonstrated high levels of CCND1 and L1CAM expression in C11orf95-RELA translocation-positive ependymomas. As CCND1 serves as a direct transcriptional target of NF-κB signaling and L1CAM is associated with aberrant cell-cell adhesion and NF- κB activation in tumors, these results suggest a role for atypical NF- κB signaling in ST-EPN. The group also demonstrated aberrant NF- κB signaling in mouse neural stem cells (NSCs) – progenitor cells that are believed to be the cells-of-origin of ependymoma. Transduction of the C11orf95-RELA fusion resulted in significant activation of NF- κB target genes relative to NSCs transduced with C11orf95 or RELA alone. To couple such findings with physiological effects *in vivo*, Parker et. Al. transduced isolated NSCs from transgenic mice with either C11orf95^{RFP}, RELA^{RFP}, or C11orf95-RELA^{RFP} retroviruses. NSCs transduced with each virus were implanted into the cerebrum of 6-week old CD1-nude mice. While mice implanted with C11orf95^{RFP} or RELA^{RFP} viruses formed very few or no brain tumors, all mice implanted with the C11orf95-RELA^{RFP} virus succumbed to brain tumors within 21 days. Brain tumors recapitulated histological findings characteristic of human ST-EPN, and demonstrated similar immunoreactivity for ST-EPN markers. In comparison to tumors of a separate mouse model of ST-EPN driven by *EPHB2*, which is not specific to C11orf95-RELA positive ST-EPN, this C11orf95-RELA mouse tumor model

exhibited marked upregulation of NF-κB genes, as shown by Ingenuity Pathway Analysis (IPA) (Parker et. Al. 2014).

While Parker et. Al. demonstrated transformation of mouse embryonic NSCs and activation of NF-κB by the C11orf95-RELA fusion *ex vivo*, in 2018 Ozawa et. Al. created a *de novo* mouse model demonstrating tumor formation and NF-κB activation *in vivo*. Their mouse model utilized the RCAS/tv-a system, a system previously developed for glia-specific gene transfer in transgenic mice. Gene set enrichment analysis (GSEA) performed by Pietsch et. Al. further support evidence for a role of aberrant NF-κB in ST-EPN tumorigenesis. In comparison to fusion-negative human ST-EPN cases, fusion positive cases exhibited significant activation of NF-κB and interferon signaling, thus demonstrating upregulation of NF-κB in human tumors.

Targeting NF-κB Subunits in Supratentorial Ependymoma

Although there is widespread evidence of NF-κB upregulation in C11orf95-RELA fusion ST-EPN tumors, the contribution made by the NF-κB dimer in aberrant NF-κB signaling has not been investigated. In vertebrates, NF-κB denotes not a single protein but a family of five transcription factors: RelA/p65, c-Rel, RelB, p52, and p50, encoded by the *rela, rel, relb, nfkb2*, and *nfkb1* genes, respectively. These transcription factors combine as homo- or heterodimers to form 15 different possible NF-κB protein dimers. All five NF-κB transcription factors share an N-terminal Rel homology domain (RHD), responsible for DNA binding, nuclear localization, and homo- and heterodimerization. In contrast, the transcriptional activation domain (TAD), which is needed for positive regulation of gene expression, is present only in RelA, c-Rel, and RelB. As they lack TADs, p50 and p52 can repress transcription when associated as homodimers or p50/p52 heterodimers. However, if associated with a TAD-containing NF-κB family member or another protein capable of coactivator recruitment, this transcriptional repression can be overridden. In addition to regulation via the presence or absence of a TAD, different NF-κB dimer

combinations have differential sequence recognition specificities and affinities for different IκB proteins, thus creating widespread variability in NF-κB signaling (Hoffman et. Al. 2006).

While support for upregulation of NF- κB signaling in ST-EPN is well documented, specifications regarding the contributions and necessities of different NF- κB subunits in driving ST-EPN tumorigenesis has not been investigated. To date, all gene expression profiling of NF- κB expression in ST-EPN has been performed using tissue from ST-EPN tumors, neglecting consideration of cell heterogeneity within the tumor. As discussed, NF- κB signaling plays a predominant role in regulation of inflammatory processes. Thus, it is unknown whether upregulation of NF- κB signaling identified in the above studies is occurring in non-oncogenic, neuroinflamatory cell populations or whether NF- κB signaling is upregulated in the oncogenic, C11orf95-RELA expressing cell population to drive tumorigenesis. With the NF- κB dimer serving as the central mediator of transcriptional regulation in the NF- κB signaling pathway, we sought to investigate the implications of the different NF- κB transcription factors within the oncogenic ST-EPN cell population in driving tumorigenesis.

Prior Models Utilized to Study Supratentorial Ependymoma

Development of supratentorial ependymoma is a highly complex process driven by a somatic gene mutation occurring in an undefined population of progenitor cells in the cerebral cortex. In order to assess if and how different NF- κB transcription factors contribute to ST-EPN tumorigenesis, a valid model that enables cell-specific and temporal control is thus required. Models of ST-EPN have progressed significantly since 2000. In 2005, Taylor et. Al. performed a combination of oligonucleotide gene expression arrays and array comparative genomic hybridization (aCGH) to show that supratentorial, posterior fossa, and spinal ependymomas possess different gene expression signatures. The differential gene expression signatures included genes regulating neural precursor cell proliferation and differentiation in the corresponding tumor region of the CNS. Specifically, supratentorial tumors expressed markedly elevated levels of members of the NOTCH and EPHB-EPHRIN cell signal systems,

which normally act to maintain normal neural stem cells in the cerebral SVZ. Interference with normal EphB-Ephrin interactions in SVZ cells of mice disrupts neuroblast chain migration and dramatically increases astrocyte proliferation, resulting in the formation of proliferative growths along the ventricle surface (Conover et. Al. 2000). Data from such gene expression profiles has been used to generate cell and animal models of ST-EPN.

In conjunction with their 2005 work, Taylor et. Al. generated a mouse model of posterior fossa ependymoma (PF-EPN) using stereotactic injections of sorted tumor cell populations. Using immunoglobulin-conjugated magnetic beads, the lab isolated cells from whole-cell populations of fresh ependymoma samples that expressed gene markers for PF-EPN. Cells were injected into the superficial cerebral cortex of 7-week-old NOD-SCID mice. Animals developed brain tumors with characteristic morphological features of ependymoma. Xenografts from the tumors further recapitulated site-specific gene expression signatures characteristic of the parent PF-EPN tumor (Taylor et. Al 2005).

In 2010, Johnson et. Al. developed the first mouse model of ST-EPN by amplification of EPHB2 in mouse forebrain neural stem cells. Analysis of DNA copy number alterations, messenger mRNA, and micro miRNA expression profiles among tumor samples segregated tumors by CNS location and identified copy number variants and alterations that might contribute to disease and clonal selection in different ependymoma subtypes. The *Ink4a/Arf* locus was found to be frequently deleted in human cerebral ependymomas, and *EPHB2* was identified as a common DNA copy number alteration - as validated by prior studies (Taylor et. Al. 2005, Poppleton and Gilbertson 2007). To develop their model, the lab isolated enhanced green fluorescent protein $(eGFP)^{+}$ cells from the cerebrum of $Ink4a/Arf^{+/+}$ and $Ink4a/Arf^{-/-}$ embryonic day 14.5 mice, and cultured the cells under conditions to promote stem cell growth. The group then challenged $Ink4a/Arf^{-/-}$ cells with Ephb2. Cultured cells were then implanted into the cerebrum of immunocompromised mice. Over 50% of mice implanted with *Ephb2* transduced embryonic cerebral $Ink4a/Arf^{-/-}$ developed brain tumors within 200 days of implantation. These tumors

were histologically similar to human ependymoma and demonstrated ultrastructural features characteristic of human ependymoma, thus establishing the first mouse model of ST-EPN (Johnson et. Al. 2010).

After identification of the C11orf95-RELA fusion in ST-EPN, Parker et. Al. furthered the Johnson mouse model using retroviruses. The group isolated NSCs from Ink4a/Arf$^{-/-}$and Blbp-eGFP transgenic mice and transduced them with a C11orf95-RELA retrovirus. NSCs transduced with the virus were then implanted into the cerebrum of female 6-week old CD1-nude mice and analyzed for tumor development. All mice implanted with NSCs containing the fusion construct developed brain tumors within 20 days. These neoplasms recapitulated histological and morphological features of ST-EPN, and expressed markers characteristic of supratentorial ependymoma (Parker et. Al. 2014).

While these models demonstrated that the C11orf95-RELA fusion can transform embryonic mouse neural stem cells *ex vivo*, until 2018, whether the fusion could drive ependymomagenesis *de novo* in the brain was publically unknown. In 2018, the Gilbertson lab developed a *de novo* mouse model using the RCAS/TVA system to deliver the C11orf95-RELA fusion into specific brain cell types in the mouse brain. Over 90% of mice injected with the fusion developed tumors within 2 months of injection. These C11orf95-RELA induced tumors displayed histological and morphological features characteristic of ependymoma, and electron microscopy and immunostaining identified several expression features common to human ependymomas (Ozawa et. Al. 2018).

Although this *de novo* mouse model demonstrated transformation of embryonic neural mouse stem cells to produce ST-EPN tumors, its ability to be utilized for additional studies of ST-EPN is limited. While the RCAS/TVA system is a versatile tool for performing lineage tracing and gene function analysis *in vivo*, the insert capacity of the virus is limited and its infection rate i*n vivo* is relatively inefficient. The insert size in RCAS systems is limited to 2.8 kB, thus limiting the genes that can be evaluated with this system and excluding the ability to study key oncogenic factors involved in human cancers. In addition, studies utilizing the RCAS system in various tissues have shown that the number of cells of the targeted tissue that become infected *in vivo* is significantly limited. This low infection rate means that only very

potent oncogenes are likely to stimulate tumor formation *in vivo*, thus limiting the specific candidate genes that can effectively be studied in specific tissues (Ahronian and Lewis, 2017).

A De Novo Mouse Model of Supratentorial Ependymoma

To circumvent these drawbacks, our lab developed a *de novo* mouse model of ST-EPN using the *piggyBac* transposase system coupled with *in utero* electroporation (IUE). The *piggyBac* transposase system has been utilized as a lineage labeling system in various tissues (Kim et. Al. 2011, Ding et. Al. 2005, Saridey et. Al 2009, Yusa et. Al. 2009). *In utero* electroporation (IUE) has been utilized as an efficient method to deliver multiple transgenes into murine neural progenitors in the developing forebrain, and in studies of neocortical development (LoTurco et. Al. 2009). In 2012, Chen and LoTurco combined a binary *piggyBac* transposon plasmid system with IUE to successfully develop a lineage and fate-mapping tool for neural progenitors (Chen and LoTurco, 2012). In addition, the CRISPR/Cas9 system can be used in combination with *piggyBac* transposase lineage labeling and IUE to induce somatic mutations in cells in neural progenitor lineages and to investigate the effects on cells in each lineage (Chen et. Al. 2015). Here, we have utilized these methods to generate a mouse model of ST-EPN that circumvents the limitations of the RCAS-TVA system.

The *piggyBac* transposase system has emerged as a promising non-viral vector system for efficient, sustained and high level transgene expression in mammalian cells (Di Matteo et. Al 2012, Ding et. Al. 2005, Saridey, Liu, and Doherty 2009). Transposons are mobile genetic elements that can be utilized to integrate transgenes into host cell genomes. The *piggyBac* transposon, originally isolated from the cabbage looper moth, Trichoplusiani, is recognized as one of the most efficient DNA transposons for the manipulation of mammalian genomes. The *piggyBac* tranposase system consists of two main components: a donor plasmid and a helper plasmid. The donor plasmid carries the gene of interest, flanked by two terminal repeat domains. The helper plasmid catalyzes the movement of the transposon (gene of interest) via the expression of its *piggyBac* transposase (PBase) (Saridey, Liu, and Doherty 2009). By placing PBase activity under the direction of cell-type specific promoters, this system can be

utilized to insert desired transposon(s) into specific cell populations. The system can be utilized with more than one donor plasmid. In this way, fluorescent constructs such as GFP and mRFP can be used in addition to other transgenes to enable lineage tracing.

ST-EPN is driven by a somatic gene mutation occurring in an undefined population of progenitor cells in the cerebral cortex. Thus, an accurate model of ST-EPN requires cellular and temporal control of transgene expression. *In utero* electroporation has emerged as an efficient method to deliver transgenes to specific populations of cerebral cortical precursor cells at select developmental time points (LoTurco, Manent, and Sidiqi 2009). *In utero* electroporation is ultimately a surgical operation whereby a pregnant mouse (embryonic day [E]9 -16) is subjected to abdominal incision for access to and exposure of all its uterine horns. Using pulled glass capillaries, desired transgenes are injected into a lateral ventricle of each embryo. After injection of the DNA solution, each brain is individually electroporated via placement between two electrode paddles on opposing hemispheres. Upon application of current pulses, transient electropores are formed within cell membranes, allowing the uptake of large molecules such as DNA into the cytoplasm (Shimogori and Ogawa, 2008). The electrode paddles have opposing charges. Application of electroporation fields moves negatively charged DNA towards the positive electrode, therefore enabling spatially directed cell transfection.

Thus, by combining the *piggyBac* transposase system with *in utero* electroporation, transgenes can be delivered to specific cerebral cortical precursor cell populations at specific developmental time points. The CRISPR/Cas9 system can layered into this system to enable time- and population-specific genome editing. The clustered regularly interspaced short palindromic repeats (CRISPR)-Cas9 system, originally identified as a mediator in adaptive immunity in bacteria and archaea, has become a powerful tool for genome engineering over the last decade. The system utilizes Cas9, an RNA-guided endonuclease that recognizes protospacer-adjacent motif sequences (PAMs), and a guide RNA (gRNA), that is complementary to the target locus. The guide RNA directs Cas9 to its specified target for specific gene ablation, given that the target has a proximal PAM sequence. The CRISPR/Cas9 system has progressed

significantly since its development, now enabling correction of genetic mutations *in vivo*, multiplex genome editing, introduction of new transgenes, and far more (Chen & LoTurco, 2012; Cong et. Al. 2013).

Here, we have used the *piggyBac* transposase system and IUE to create a novel mouse model of ST-EPN. This model recapitulates morphological and genetic profiling characteristics of human ST-EPN, as demonstrated by histology and gene expression analysis. The cell-specific and temporal control provided by the model allows for an assessment of how different NF- κB transcription factors contribute to ST-EPN tumorigenesis by targeting NF- κB within the oncogenic ST-EPN cell population. Current literature demonstrates a role of the NF- κB pathway in ST-EPN tumorigenesis. However, the specific contribution of the different NF-κB transcription factors in driving tumorigenesis within the oncogenic ST-EPN cell population has not been investigated. Seeing as the p50 NF- κB transcription factor lacks a TAD domain, we hypothesize that overexpression of this gene will attenuate ST-EPN tumorigenesis by preventing transcriptional activation of target genes involved in ST-EPN oncogenesis.

METHODS

Plasmid Construction

Plasmids were constructed for development of an ST-EPN mouse model. To make pPBCAG-FUS1-HA, pPBCAG-RELA-HA, pPBCAG-p50-Flag, and pPBCAG mCherry, N-terminal HA-tagged C11orf95-RELA fusion (termed FUS1), HA-tagged RELA, Flag-tagged p50, and mCherry sequences, respectively, were amplified and replaced the eGFP cassette of a previously constructed pPBCAG-eGFP construct. Replacement was achieved using the *EcoRI* and *Not1* sites of the original plasmid. For construction of pCAG-PBase, the PBase coding sequence was directly inserted downstream of the CAG promoter, a gift from Fuyi Chen.

Cell Culture Transfection

Hek293T cells were plated 24 hours prior to transfection in a 12-well plate (~ 150 – 200K cells/well). Cells were transfected at 70 – 80% confluency with plasmids diluted to 1.0 µg/µL prior to transfection. Upon starting the transfection protocol, media was aspirated and replaced with 1 mL of fresh media. Transfection was accomplished using the Lipofectamine LTX w/PLUS Transfection protocol. Cells were harvested at 37C overnight and harvested 24 hours post-transfection. To harvest, cells were washed with 1X PBS and incubated with 4% PFA (4% paraformaldehyde/PBS) at room temperature for 20 minutes. Cells were washed 3X with 1x PBS and prepared for immunocytochemistry.

Immunocytochemistry

Fixed Hek293T cells were incubated with blocking buffer (7.5% goat serum, 0.1% Triton-X 100 in 1X PBS) for 1 hour at room temperature. Cells were washed 3X with 1x PBS, and incubated with primary antibody in antibody buffer (10% goat serum, 0.05% Triton-X 100 in 1x PBS) for 2 hours at room temperature. The following primary antibodies were used: Mouse anti-HA (1:1000, Invitrogen), Rabbit anti-V5 (1:1000, Invitrogen), and Mouse anti-Flag (1:1000; NE BioLabs). Following incubation, cells were washed 3x with 1x PBS and incubated with secondary antibody for 2 hours at room temperature in antibody buffer. The following secondary antibodies were utilized: Goat anti-Rabbit Alexa Fluor® Plus 647 (1:1000, Invitrogen), Goat anti-Mouse Alexa Fluor® Plus 488 (1:1000, Invitrogen). After incubation, cells were rinsed 1x with 1x PBS and incubated with 4-6-diaminodino-2-phenylindole (1:2000, DAPI, Invitrogen) for 20 minutes in antibody buffer at room temperature for nuclear staining. Cells were washed 3x with 1x PBS and coverslips were mounted on slides for imaging on a Leica TCS Sp8 Confocal microscope.

Colocalization Analysis

Single cell high magnification images were acquired on a Leica TCS SP8 Confocal microscope at 63X. Nuclear regions were drawn free-hand to designate the region of interest for colocalization analysis

via Coloc2 of the ImageJ imaging software, which was set to perform pixel intensity correlation over space methods of Pearson. Threshold pixel intensity was set to minimum of 0 pixels. Pearson's R values of n = 6 cells were averaged to obtain assessments of protein colocalization.

Animals

CD1 mice were obtained from Charles River Laboratories, Inc. (Wilmington, MA), and maintained at the University of Connecticut vivarium. Animal gestation ages were determined and confirmed during surgery. Both male and female embryos were used for surgery, and all procedures and experimental approaches were approved by the University of Connecticut IACUC.

In Utero Electroporation

In utero electroporation was performed as previously described [28, 29]. Briefly, mice were anesthetized with a mixture of ketamine/xylazine (100/10 mg/kg i.p.). Metacam analgesic was administered daily at dosage of 1 mg/kg sub cutaneously at 24 and 48 hours following surgery. To visualize the plasmid during electroporation, plasmids were mixed with 2 mg/ml Fast Green (Sigma). In all conditions described, pPBCAG-FUS1-HA, pPBCAG eGFP, pPBCAG mCherry, and the helper plasmid CAG-PBase were used at the final concentration of 1.0 µg/µL. pPBCAG-RELA-HA, pPBCAG-p50-Flag, and PX330-p50 were used at a final concentration of 1.5 µg/µL. Electroporation was performed at embryonic day 12 or 14 (E12 or E14). During surgery, the uterine horns were exposed and one lateral ventricle of each embryo was pressure injected with 1–2 µl of plasmid DNA. Injections were made through the uterine wall and embryonic membranes by inserting a pulled glass microelectrode (Drummond Scientific) into the lateral ventricle and injecting by pressure pulses delivered with a Picospritzer II (General Valve). Electroporation was accomplished with a BTX 8300 pulse generator (BTX Harvard Apparatus) and BTX tweezertrodes. A voltage of 65–75V was used for electroporation.

Immunohistochemistry

Animals were deeply anesthetized with isoflurane and perfused transcardially with 4% paraformaldehyde/PBS (4% PFA). Brain samples were post fixed for 24 hours in 4% PFA and sectioned at 65µm thickness on a vibratome (Leica VT 1000S). Sections were processed as free-floating sections. After blocking in PBS containing 5% normal goat serum (Sigma) and 0.3% Triton X-100 (Sigma) for 2 hours at room temperature, tissue sections were incubated with primary antibodies overnight at 4 ◦C in the blocking solution. The following primary antibodies were used (separately): rabbit anti-HA (1:1000, Invitrogen), and rabbit anti-V5 (1:1000, Invitrogen). Tissue sections were washed in PBS, incubated with the appropriate secondary antibodies (Goat anti-Rabbit Alexa Fluor 647; 1:2000, Invitrogen), for 2 hours at room temperature and washed in PBS. Nuclei were labeled 4-6-diaminodino-2-phenylindole (1:2000, DAPI, Invitrogen). Whole brain and high magnification images were acquired on a Leica TCS SP8 confocal system.

Tumor Area Analysis

Transfected and/or tumor regions were imaged on a Leica TCS Sp8 confocal microscope and processed using FIJI Imaging software. Tumor nodules were outlined free-hand to create a region of interest for tumor area analysis. In brains containing more than one tumor nodule, nodules were assessed separately and their measurements summed to obtain total area. Total of n = 6 brains were analyzed for each condition.

RESULTS

Upregulation of the NF- κB pathway in ST-EPN is well supported in the literature (Pietsch et. Al. 2014; Parker et. Al. 2014; Gilbertson et. Al. 2018). However, whether the ST-EPN C11orf95-RELA fusion interacts with the different NF- κB transcription factor subunits in the oncogenic ST-EPN cell population is unknown. This prompted us to investigate the biochemical interactions of C11orf95-RELA with the five different NF-κB subunits: RelA, RelB, c-Rel, p50, and p52. Generation of p50 is accomplished via endoproteolytic cleavage of the precursor, p105. Similarly, p52 is generated from its precursor protein, p100. To account for the potential that the C11orf95-RELA fusion interacts with p50 and/or p52 prior to protein processing, we therefore also tested for the interaction of C11orf95-RELA with p105 and p100. Hek293T cells were transfected with an HA-tagged fusion construct. Following immunoprecipitation, blots were stained to detect each of the NF- κB subunits: RelB, c-Rel, p50, p52, the p50 precursor p105, and the p52 precursor p100. All NF- κB subunits were detected in whole cell lysate (WCE) and the C11orf95-RELA fusion co-immunoprecipitated with RelB, c-Rel, p50, and p105. We also previously developed various fusion mutants containing mutations or deletions in various regions of the C11orf95 domain. These mutants included a fusion with a mutation in the zinc finger domain of C11orf95 (HA-FUS1-ZFD-ΔAA) and a mutant comprised of the fusion with a deletion of one of the nuclear localization sequences in C11orf95 (HA-FUS1-NLS-Del). Both mutants demonstrated interaction with NF- κB subunits RelB, cRel, p50, and p105 (Figure 1). These results show that the C11orf95-RELA fusion is capable of interacting with other NF κB subunits, thus supporting a potential role for aberrant NF- κB signaling in driving ST-EPN tumorigenesis.

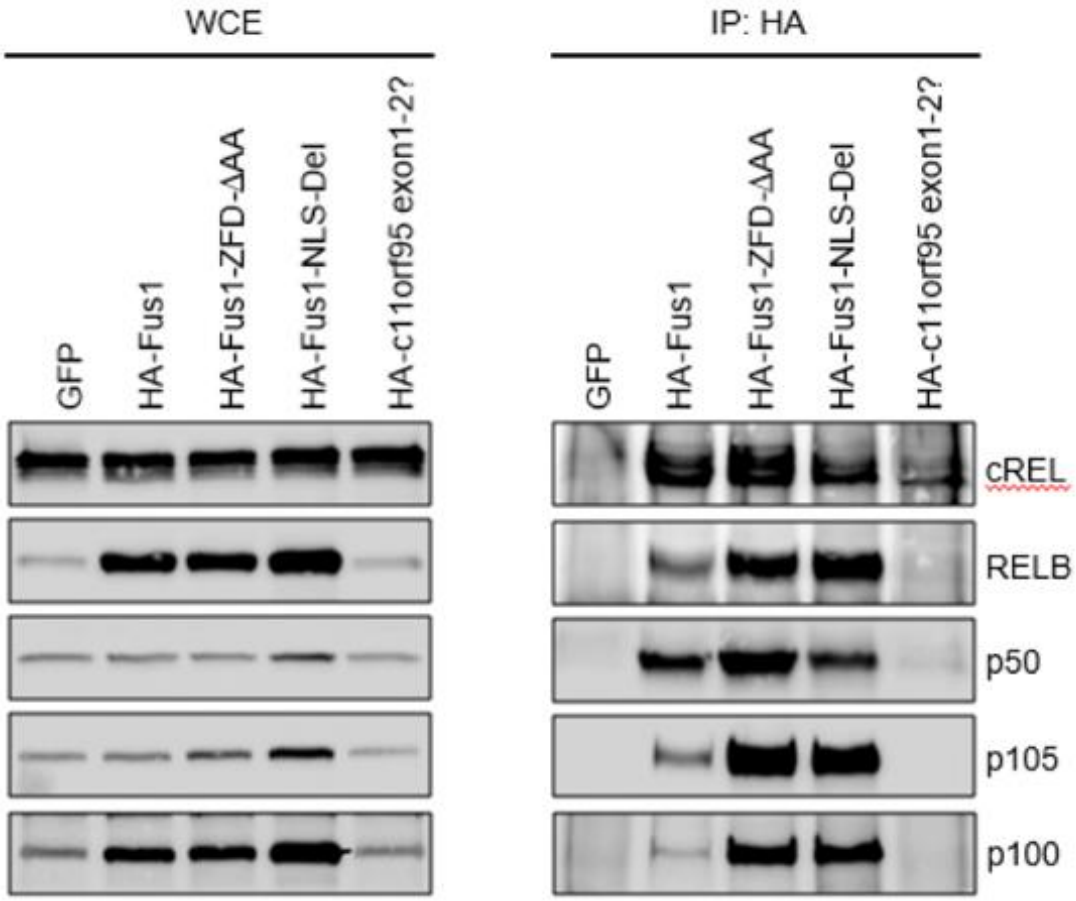

Figure 1: NF-kβ Subunits Interact with C11orf95-RELA Fusion *in vitro*

Pull down of Hek293T cells transfected with an HA-tagged C11orf95-RELA fusion construct. All NF- κB subunits were detected in whole cell lysate (WCE) and immunoprecipitated C11orf95-RELA fusion stained positively for RelB, c-Rel, p50, p105, and p100. Fusion mutants containing a fusion with a mutation in the zinc finger domain of C11orf95 (HA-FUS1-ZFD-ΔAA) and a mutant comprised of the fusion with a deletion of one of the nuclear localization sequences in C11orf95 (HA-FUS1-NLS-Del) both demonstrated interaction with NF- κB subunits RelB, cRel, p50, p105, and p100. Data provided in collaboration with Jianguo Wu.

Next, we looked to see where the fusion and NF- κB proteins were localizing within cells. We developed differentially tagged constructs – an HA-tagged C11orf95-RELA fusion plasmid, a V5-tagged C11orf95-RELA fusion plasmid, an HA-tagged RELA plasmid, and a Flag-tagged p50 plasmid. Hek293T cells were transfected with C11orf95-RELA-HA, RELA-HA, or p50-Flag constructs and imaged at high magnification to assess the cytoplasmic vs. nuclear localization of each protein. All proteins localized to cell nuclei, showing no positive staining in the cytoplasm (Supplemental Figure 1). To gain insight into whether these constructs may be localizing to similar regions within the nucleus to influence gene expression, we then sought to assess the degree of colocalization of the proteins within cell nuclei. Hek293T cells were co-transfected with the following combinations: HA-tagged C11orf95-RELA and V5-tagged C11orf95-RELA, V5-tagged C11orf95-RELA and HA-tagged RELA, or HA-tagged C11orf95-RELA and Flag-tagged p50. Following immunostaining, single cell nuclei were imaged (Figure 2A) and the degree of colocalization was quantified using the Coloc2 add-on of the FIJI imaging software. Analysis of pixel intensity colocalization demonstrated that the C11orf95-RELA fusion demonstrates positive nuclear colocalization with itself, with an average Pearson's R value of 0.837 ± 0.0564. Similarly, the C11orf95-RELA fusion demonstrates positive nuclear colocalization with RELA (Avg. Pearson's R Value = 0.745 ± 0.0957). In contrast, the C11orf95-RELA fusion demonstrated no significant correlation in nuclear colocalization with p50 (Avg. Pearson's R Value = -0.130 ± 0.3005) (Figure 2B). These results suggest that the C11orf95-RELA fusion may be capable of homodimerization. They also demonstrate that RelA and C11orf95-RELA have similar nuclear localization patterns, suggesting that RelA and C11orf95-RELA may have similar DNA binding sites, and/or that the C11orf95-RELA fusion is capable of heterodimerizing with RELA to influence gene expression. In conjunction with our findings that C11orf95-RELA interacts with p50 (Figure 1), this data suggests that while C11orf95-RELA interacts with p50, p50 also localizes to different nuclear locations independently of dimerization with C11orf95-RELA.

A

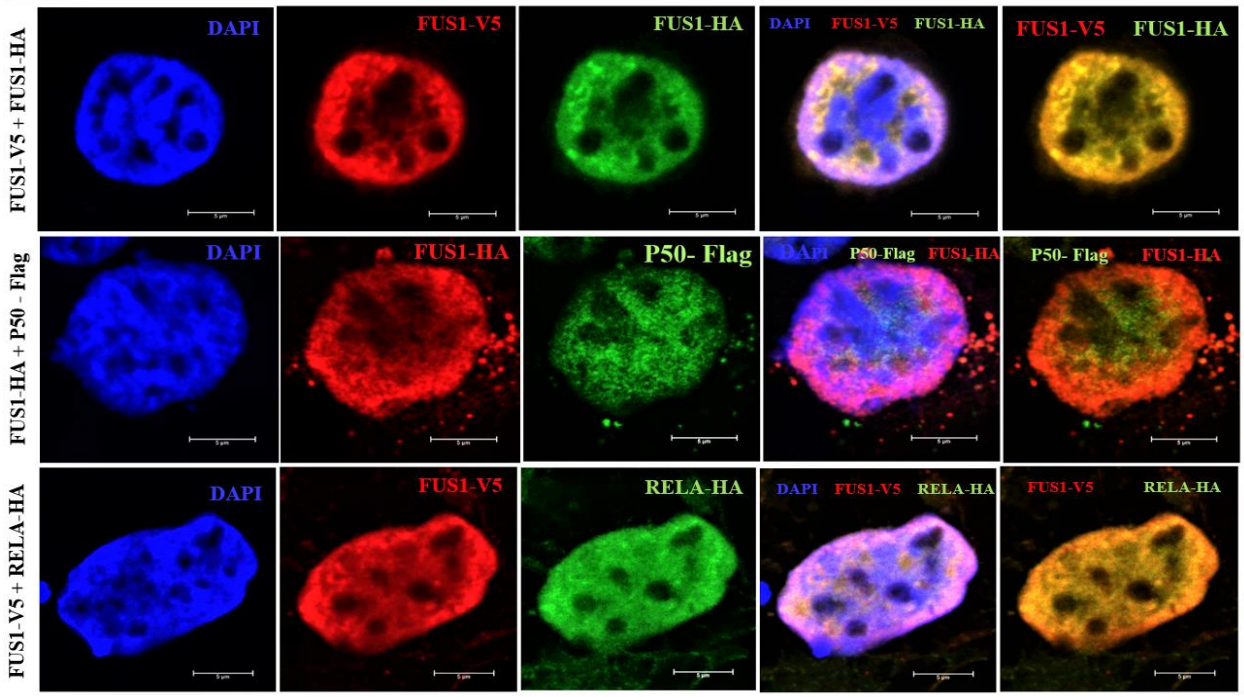

B

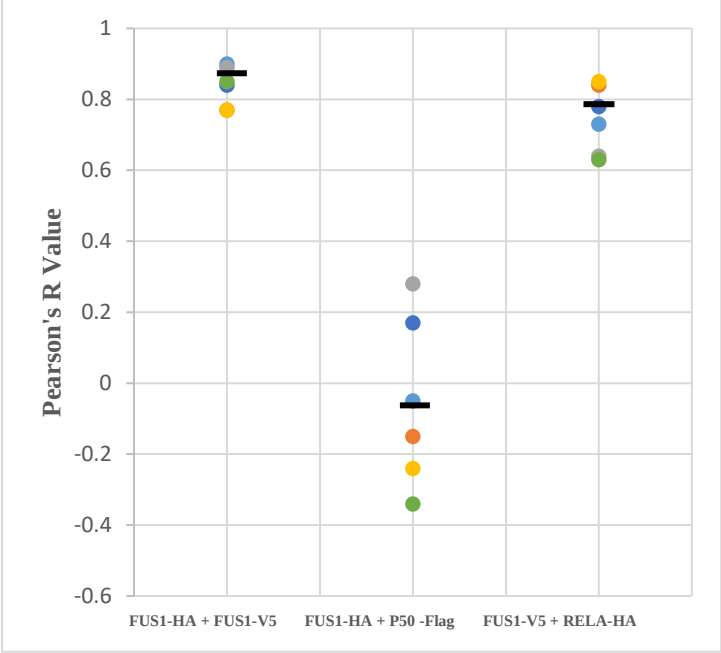

	FUS1-V5 + FUS1-HA	*FUS1-HA + P50-Flag*	*FUS1-V5 + RELA-HA*
	0.9	-0.5	0.73
	0.77	-0.15	0.84
	0.89	0.28	0.64
	0.77	-0.24	0.85
	0.84	0.17	0.78
	0.85	-0.34	0.63
Average Pearson's R Value	**0.837** ± 0.0564	**-0.13** ± 0.3005	**0.745** ± 0.0957

Figure 2: C11orf95-RELA Demonstrates Better Nuclear Colocalization with other C11orf95-RELA Constructs and RelA than p50 in Hek293T Cells

(A) Representative images of nuclear colocalization in Hek293T cells co-transfected with: FUS1-V5 and FUS1-HA, FUS1-HA and p50, or FUS1-V5 and RELA-HA. Scale bar = 5 µm.
(B) Quantitative colocalization analysis of Hek293T cells transfected with: FUS1-V5 and FUS1-HA, FUS1-HA and P50-Flag, or FUS1-V5 and RELA-HA (n = 6 cells in each transfection condition).

Biochemical analysis demonstrated interaction of C11orf95-RELA with p50 and RELA. To assess potential functional *in vivo* effects due to C11orf95-RELA interaction with NF-κB subunits RelA and/or p50, we developed a *de novo* mouse model of ST-EPN, as previously described. Following *in utero* electroporation at E12 – E14, all mice were harvested between P14 and P21 to assess for tumor presence and size. Only brains demonstrating successful transfection (via GFP signal) were utilized for analysis. Transfected brain slices were stained with 4-6-diaminodino-2-phenylindole to visualize tumor nodules, and imaged on a Leica TCS Sp8 Confocal microscope (Figures 3A and 4A).

Images were processed using FIJI imaging software to quantify tumor area (n = 5 - 9 brains per condition). Animals expressing the C11orf95-RELA fusion alone had an average tumor area of 3,320,253 ± 2,128,305 μm^2. Those with C11orf95-RELA and overexpression of p50 had an average tumor area of 3,974,786 ± 1,850,118 μm^2, and those with C11orf95-RELA and knock-out of p50 had an average tumor area of 798,169.4375 ± 442,096 μm^2. In comparison to WT C11orf95-RELA-HA, tumor area was unchanged in C11orf95-RELA-HA + P50-Flag animals but was significantly reduced in C11orf95-RELA-HA + P50 CRISPR animals (Figure 3B). In fact, some C11orf95-RELA-HA + P50 CRISPR animals failed to generate tumors at all. In contrast, animals with C11orf95-RELA and overexpression of RELA had an average tumor area of 17,856,057 ± 5,097,949 μm^2. Tumor area was significantly increased in C11orf95+RELA-V5 + RELA-HA animals in comparison to control (Figure 4B). Animals expressing P50 or P50 CRISPR without the C11orf95-RELA fusion failed to produce tumors, and were not included in the tumor area analysis (Supplemental Figure 2).

A

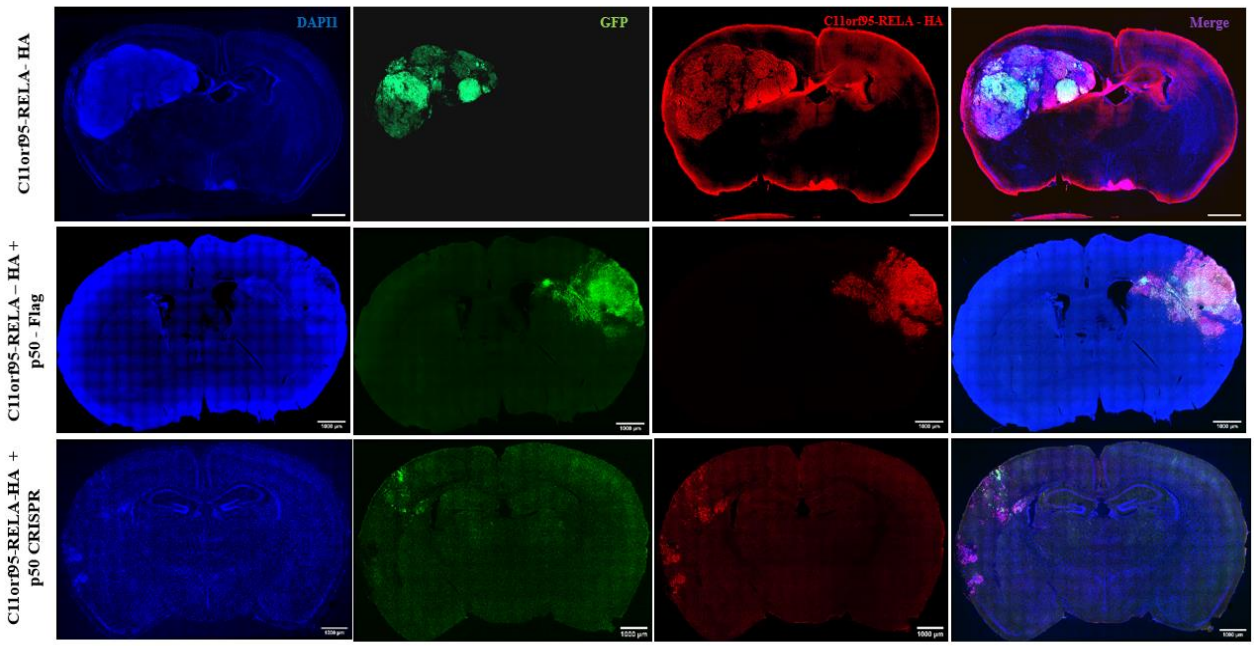

B

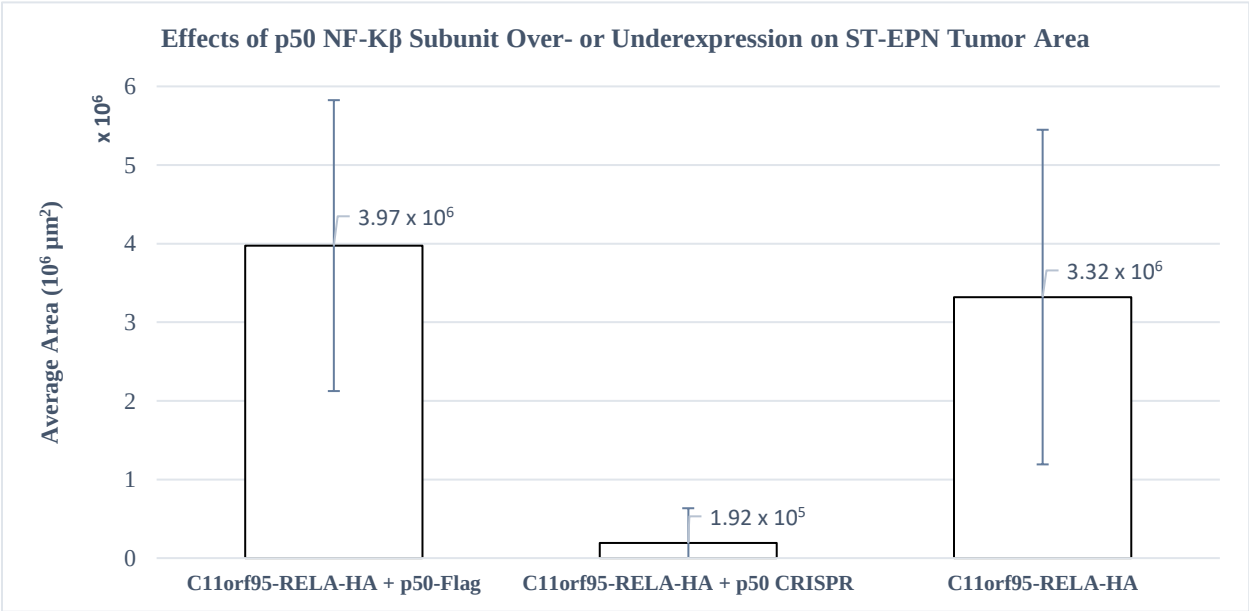

Figure 3: Knockdown of NF-κB Subunit p50 in Conjunction with WT C11orf95-RELA Fusion Reduces Ependymoma Tumor Size

(A) Representative images of tumors generated from WT HA-tagged C11orf95-RELA fusion transfected mice, HA- tagged C11orf95-RELA with overexpression of p50, and HA-tagged C11orf95-RELA with CRISPR/Cas9 knockdown of p50 (top to bottom). All brains were harvested at P21. Scale bar = 1000 µm.

(B) Quantification of tumor area in μm^2. n = 6 brains in C1orf95-RELA-HA, n = 9 brains in C11orf95-RELA-HA + p50-Flag, n = 5 brains in C11orf95-RELA + p50 CRISPR.

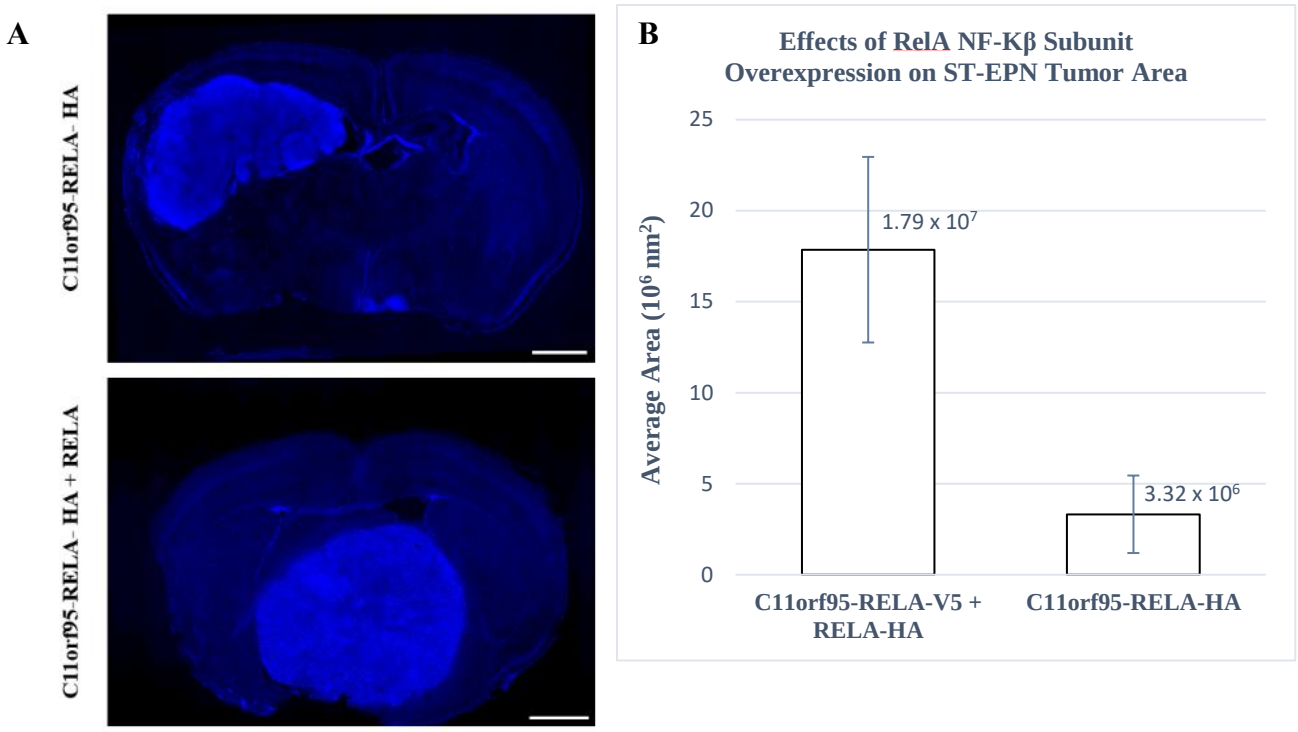

Figure 4: Overexpression of NF-κB Subunit RelA in Conjunction with WT C11orf95-RELA Fusion Increases Ependymoma Tumor Size

(A): Representative images of tumors generated from WT HA-tagged C11orf95-RELA fusion transfected mice (top) and V5- tagged C11orf95-RELA with overexpression of RelA (bottom). All brains were harvested at P21. Scale bar = 1000 μm.

(B) Quantification of tumor area in μm^2. n = 6 brains in each condition.

While average tumor area was unchanged in C11orf95-RELA-HA + p50-Flag animals, it was clear that transfected cell morphology was significantly altered. We thus investigated the ability of our various constructs to alter ST-EPN cell morphology. Images of P14 - 21 animals were taken on a Leica TCS Sp8 Confocal microscope at 40X and 63X to gain insight into cell cluster and single cell morphology. Qualitatively, C11orf95-RELA animals demonstrated characteristic well circumscribed tumor boundaries with rounded, well defined cell morphology. This phenotype was reproduced in C11orf95-RELA-V5 + RELA-HA animals. In contrast, C11orf95-RELA-HA + p50-Flag tumors displayed string-like, not well-defined borders composed of filamentous cells with numerous processes (Figure 5, Figure 6A). Animals expressing Flag-tagged p50 or p50 CRISPR without the C11orf95-RELA fusion exhibited normal astrocyte and neuronal morphology (Supplemental Figure 3). Interestingly, while C11orf95-RELA-HA + P50 CRISPR animals did not demonstrate development of tumors (Figure 3A, B, Figure 5), transfected cells demonstrated cell morphology characteristics of both normal astrocytes and those found in p50-overexpressing animals (Figure 6B).

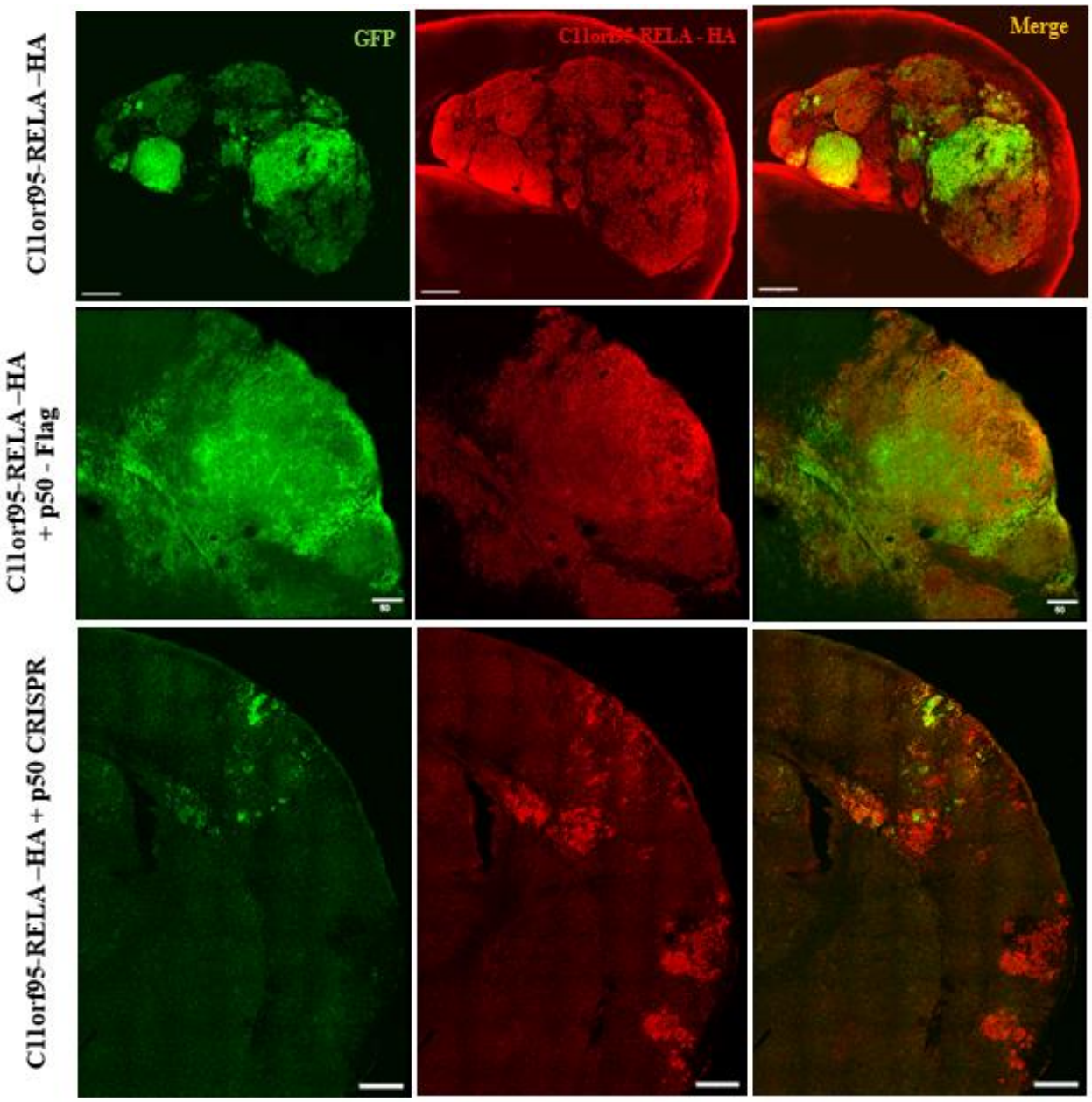

Figure 5: Overexpression of p50 Alters Neoplasm Morphology

(A) The WT fusion mutation generates tumors with well-defined borders and nodular morphology. In comparison, overexpression of p50, in conjunction with the WT C11orf95-RELA fusion, generates neoplasms with poorly defined tumor boundaries and altered cell morphology. Knockdown of p50 via CRISPR/Cas9, in conjunction with the WT C11orf95-RELA fusion, does not inhibit proliferation. However, proliferative masses are smaller in size in comparison to age-matched controls and tumor nodules are dominated by C11orf95-RELA fusion-expressing cells. Scale bar = 500µm.

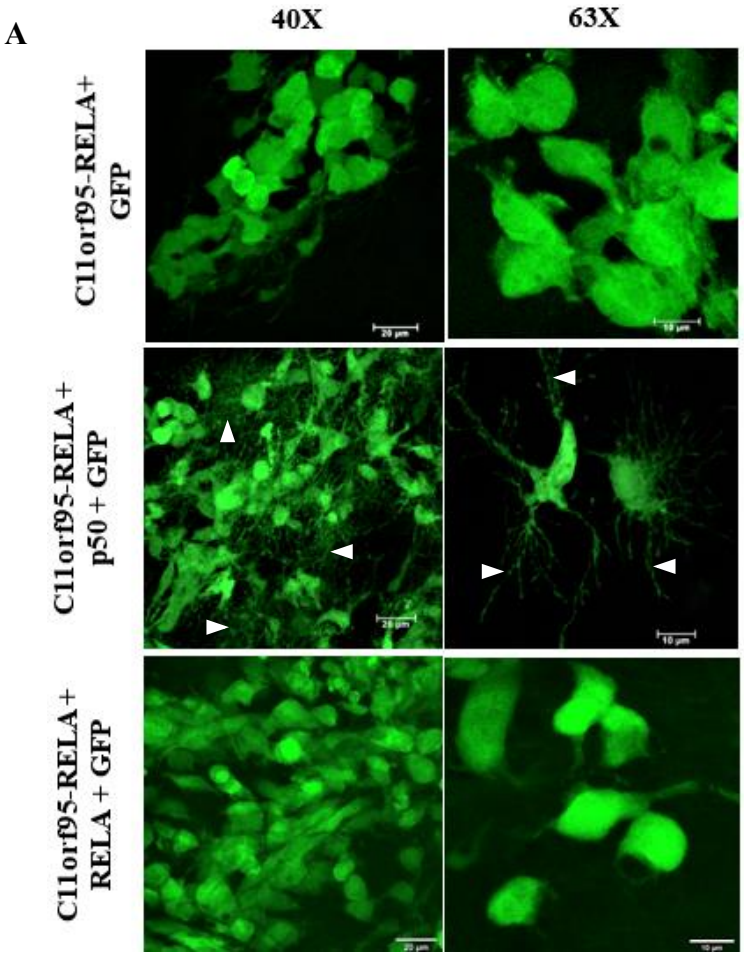

Figure 6: Overexpression of p50, but not RelA, Alters Transfected Cell Morphology of Tumors

(A) Overexpression of p50 in conjunction with the C11orf95-RELA fusion generates transfected cells that are morphologically distinct from WT C11orf95-RELA. In contrast to the well-defined, rounded morphology of WT transformed cells, transformed cells generated from p50 overexpression have extensive filamentous processes (arrow heads). Overexpression of RELA with the WT C11orf95-RELA fusion generates transformed cells with similar well-circumscribed cell borders and minimal cell processes.

(B) C11orf95-RELA-HA + P50 transfected cells demonstrated cell morphology characteristics of both normal astrocytes and those found in p50-overexpressing animals (arrow heads).

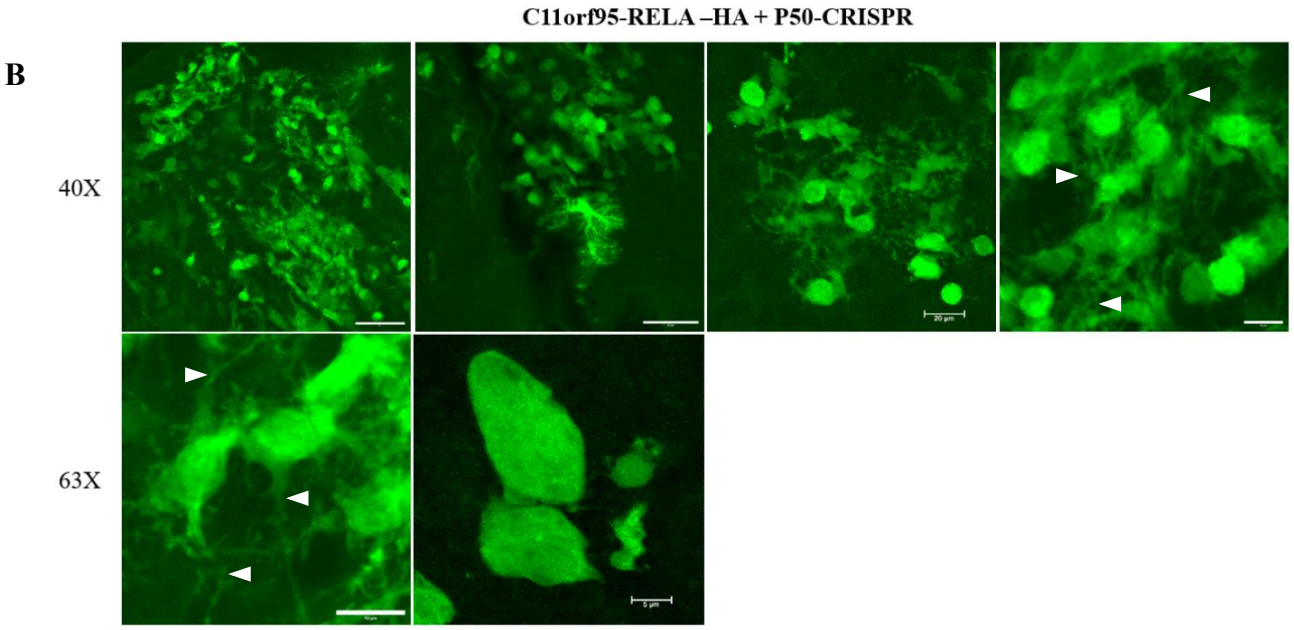

DISCUSSION

The composition of the NF- κB dimer influences its ability to recognize different DNA target sequences. Each dimer combination has varying sequence recognition specificities. Thus, transcriptional specificity is influenced by NF- κB dimer structure. The implications of this are supported in an assessment of our colocalization studies. C11orf95-RELA did not colocalize with p50 as well as it did with RELA or other C11orf95-RELA constructs. Endogenous p50-RELA or p50-p50 dimers may localize to different locations within the genome than when in association with the C11orf95-RELA fusion as Fusion-p50 dimers. In contrast, there was significant colocalization with RelA and C11orf95-RELA. This could be a result of endogenous RelA binding to similar genomic targets as the C11orf95-RELA fusion, and not necessarily due to Fusion-RelA interaction. This possibility is supported by the fact that the C11orf95-RELA fusion has the same TAD domain as does endogenous RelA. In comparison, p50 entirely lacks a TAD domain, which may play a role in generating the differential genomic target sequences. This suggests that our colocalization results may be explained by genomic interactions of p50 and RelA with their target sites in addition to effects of molecular interactions with C11orf95-RELA.

It is interesting to note that while C11orf95-RELA-HA + p50 CRISPR animals demonstrated a reduction in tumor size, cells exhibited altered morphology similar to that found in C11orf95-RELA-HA + p50-Flag animals. Various interpretations for these seemingly conflicting findings are possible. It is possible that cells with altered morphology comprise a lineage derived from a cell that failed to take up the p50 CRISPR construct during transfection. It is also possible that the cells expressing altered morphology are slowly growing tumor-like cells that will never form tumors (i.e. tumors stunted in growth). Testing the former hypothesis would require further work utilizing a p50 antibody to determine whether p50 is expressed in altered cells. Testing of the later could be performed with a developmental time course to assess tumor development over time.

The *in vitro* results of this study demonstrate that there is an interaction between the NF-κB subunits p50 and RelA with the ST-EPN fusion C11orf95-RELA. The *in vivo* results demonstrate that

these interactions have functional consequences on ST-EPN tumor development and cell morphology. How p50 and/or RelA over-and underexpression impact NF-κB dimerization at the cellular level can be utilized to summarize the functional effects identified in this study (Figure 7).

Overexpression of RELA generates larger ST-EPN tumors, while overexpression of p50 creates tumors with altered cell morphology. In contrast, knockdown of p50 reduces tumor size. In C11orf95-RELA animals alone, the oncogenic cell population can be hypothesized to comprise a mixture of Fusion-Fusion, Fusion-p50, and Fusion-RELA dimers. In C11orf95-RELA-HA + p50-Flag cells, there may be an increased proportion of Fusion-p50 and p50-p50 dimers, while C11orf95-RELA-V5 + RELA-HA cells may possess a greater proportion of Fusion-RELA and RELA-RELA dimers. In cells expressing C11orf95-RELA-HA with a CRISPR knockdown of p50, there may be few Fusion-p50 dimers and a greater proportion of Fusion-Fusion dimers. This suggests that RELA-Fusion and p50-Fusion dimers are necessary for tumor formation, and that Fusion-Fusion dimers may not have high oncogenic capacity.

Further studies investigating the functional effects of RelA knockdown are needed assess the oncogenic capacity of RelA in driving ST-EPN. To gain further insight into the mechanisms of ST-EPN tumorigenesis, identification of the transcriptional targets of the C11orf95-RELA fusion are needed. If and how these targets change with overexpression or knockdown of p50 or RelA would be useful in gaining further insight into the functional results identified in these studies, and would greatly aid in our understanding of ST-EPN tumorigenesis.

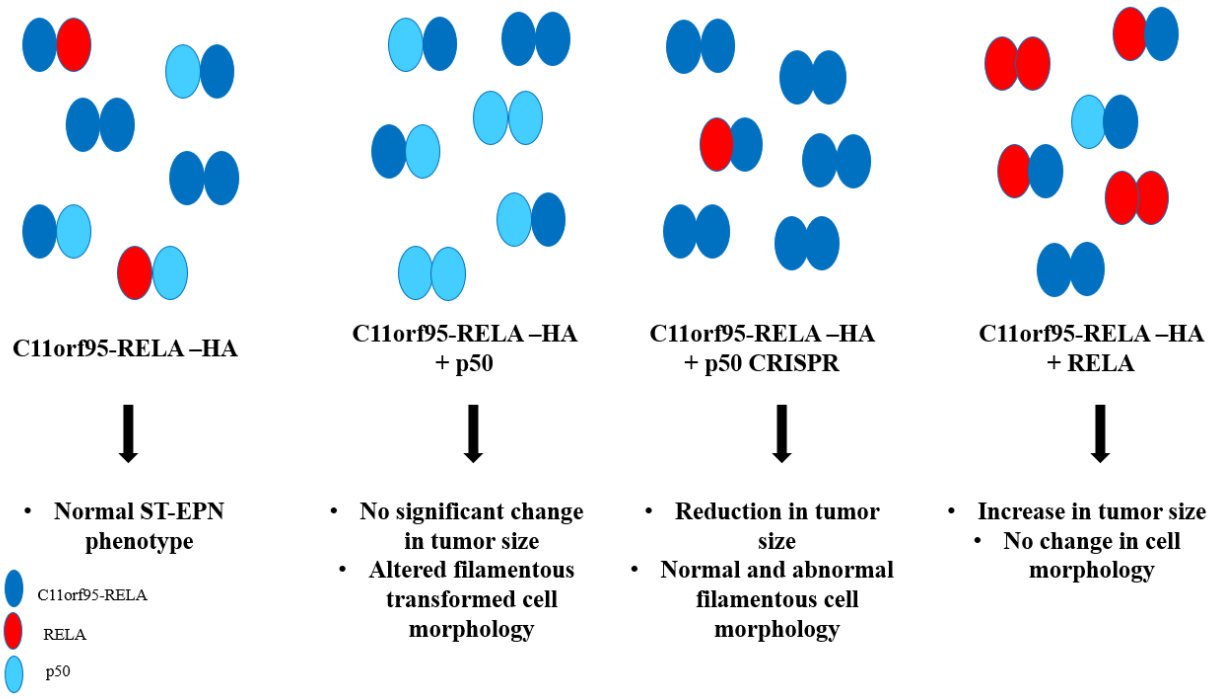

Figure 7: Schematic Representation Demonstrating Potential Effects of RelA and p50 Manipulation on NF-κB Dimerization and ST-EPN Phenotype

In comparison to WT C11orf95-RELA, overexpression of p50 may create a larger proportion of p50-Fusion and p50-p50 dimers, while knockdown of p50 reduces formation of such dimers, leading to a greater proportion of fusion-fusion dimers. Similarly, overexpression of RelA along with C11orf95-RELA may lead to a greater proportion of RelA-Fusion dimers. Coupled with the phenotypic results identified in this study, this suggests that Fusion-p50 and/or Fusion-RelA dimers are necessary for tumor formation, and that Fusion-Fusion dimers may not have high oncogenic capacity.

REFERENCES

Amirian ES, Armstrong TS, Aldape KD, Gilbert MR, Scheurer ME. (2012). Predictors of survival among pediatric and adult ependymoma cases: a study using Surveillance, Epidemiology, and End Results data from 1973 to 2007. *Neuroepidemiology*. **39**(2): 116–124.

Aschero S, Vallero S, Morra I, et al. (2010). A complex karyotype including a t (2;11) in a paediatric ependymoma: case report and review of the literature. *J Neurooncol*. **99**(1):141-146.

Chen, F. and LoTurco, J. (2012). A method for stable transgenesis of radial glia lineage in rat neocortex by piggyBac mediated transposition. *J. Neuroscience Methods* **207**: 172 – 180.

Cong et. Al. (2013). Multiplex Genome Engineering Using CRISPR/Cas Systems. *Science*. **339**(6121): 819 – 823.

Conover, J.C., Doetsch, F., Garcia-Verdugo, J.M., Gale, N.W., Yancopoulos, G.D., and Alvarez-Buylla, A. (2000). Disruption of Eph/ephrin signaling affects migration and proliferation in the adult subventricular zone. *Nat. Neurosci.* **3**, 1091–1097.

Courtois G, Gilmore TD (2006). Mutations in the NF- κB Signaling Pathway: Implications for Human Disease. *Oncogene* **12**:6831 – 6843.

de Bont JM, Packer RJ, Michiels EM, et al. (2008). Biological background of pediatric medulloblastoma and ependymoma: a review from a translational research perspective. *Neuro Oncol.* **10**(6):1040-1060.

Di Matteo M, Matrai J, Belay E, Firdissa T, Vandendriessche T, Chuah MK. (2012). PiggyBac toolbox. *Methods Mol Biol*. **859**: 241 – 254.

Ding et. Al. (2005). Efficient Transposition of the piggyBac (PB) Transposon in Mammalian Cells and Mice. *Cell* **122**: 473 – 483.

Dwyer et. Al. (2016). Neural Stem Cells to Cerebral Cortex: Emerging Mechanisms Regulating Progenitor Behavior and Productivity. *Journal of Neuroscience* **36**(45): 11394 – 11401.

Flucke U, Tops BB, de Saint Aubain Somerhausen N, Bras J, Creytens DH, Küsters B, Groenen PJ, Verdijk MA, Suurmeijer AJ, Mentzel T (2013) Presence of C11orf95–MKL2 fusion is a consistent finding in chondroid lipomas: a study of eight cases. *Histopathology* **62**:925–930.

Johanna Napetschnig and Hao Wu. (2013). Molecular Basis of NF-κB Signaling. *Annu. Rev. Biophys.* **23**: 443-468.

Kilday JP, Rahman R, Dyer S, et al. (2009). Pediatric ependymoma: biological perspectives *Mol Cancer Res*. **7(**6): 765 -786.

Kim A, Pyykko I. (2011). Size Matters: Versatile Use of PiggyBac Transposons as a Genetic Manipulation Tool. *Mol Cell Biochem* **354**: 301 – 309.

Korshunov A, Witt H, Hielscher T, et al. (2010). Molecular staging of intracranial ependymoma in children and adults. *J Clin Oncol*. **28**(19):3182 - 3190.

Leanne G Ahronian and Brian C. Lewis. (2017). Using the RCAS-TVA System to Model Human Cancer in Mice. *Cold Spring Harbor Protoc*; 1128 – 1135.

LoTurco, J. Manent, J.-B. and Sidiqi, F. (2009). New and improved tools for in utero electroporation studies of developing cerebral cortex. *Cereb. Cortex* **19** Suppl 1, i120-i125.

Mack SC, Taylor MD. (2009). The genetic and epigenetic basis of ependymoma. *Childs Nerv Syst.* **25**(10):1195-1201.

Morest, D. Kent and Silver, Jerry (2003). Precursors of Neurons, Neuroglia, and Ependymal Cells in the CNS: What Are They? Where Are They From? How Do They Get Where They Are Going? *Glia* **43**(1): 6 – 18.

Ozawa et. Al. (2018). A De Novo Mouse Model of C11orf95-RELA Fusion-Driven Ependymoma Identifies Driver Functions in Addition to NF-κB. *Cell Reports* **23**: 3787–3797.

Parker. Et. Al. (2014). *C11orf-RELA* Fusions Drive Oncogenic NF- κB Signaling in Ependymoma. *Nature* **506**: 451 – 455.

Pietsch et. Al. (2014). Supratentorial ependymomas of Childhood Carry *C11orf95-RELA* Fusions Leading to Pathological Activation of the NF- κB Signaling Pathway. *Acta, Neuropathol*. **127**: 609-611.

Rodriguez D, Cheung MC, Housri N, Quinones-Hinojosa A, Camphausen K, Joniaris LG. (2009). Outcomes of malignant CNS ependymomas: an examination of 2408 cases through the Surveillance, Epidemiology, and End Results (SEER) database (1973 – 2005). *J Surg Res*. **156**(2): 340 – 351.

Saridey SK, Liu L, Doherty JE, et. Al. (2009). PiggyBac Transposon-based Inducible Gene Expression in vivo After Somatic Cell Gene Transfer. *Mol Ther* **17**: 2115 – 2120.

Taylor et. Al. (2005). Radial Glia Cells are Candidate Stem Cells of Ependymoma. *Cancer Cell*. **8**: 323 – 335.

Tomomi Shimogori & Masaharu Ogawa. (2008). Gene application with *in utero* electroporation in mouse embryonic brain. *Develop. Growth Differ*. **50**: 499 – 506.

Vera-Bolanos E, Aldape K, Yuan Y, et al. (2015). Clinical course and progression-free survival of adult intracranial and spinal ependymoma patients. *Neuro Oncol.*; **17**(3):440–447.

von Haken MS, White EC, Daneshvar-Shyesther L, et al. (1996). Molecular genetic analysis of chromosome arm 17p and chromosome arm 22q DNA sequences in sporadic pediatric ependymomas [J]. *Genes Chromosomes Cancer.* **17**(1):37-44.

Wu, J. Armstrong, Terri S. and Gilbert, Mark R. (2016). Biology and management of ependymomas. *Neuro-Oncology* **18**(7): 902-913.

Xie TX, Xia Z, Zhang N, Gong W, Huang S (2010). Constitutive NF-kappaB activity regulates the expression of VEGF and IL-8 and tumor angiogenesis of human glioblastoma. *Oncol Rep* **12**:725–732.

Yao, Y, Mack, SC, and Taylor, MD. (2011). Molecular genetics of ependyoma. *Chinese Journal of Cancer* **30**(10): 669 – 681.

Yusa, K, Rad R, Takena J, Bradey A. (2009). Generation of Transgene-Free Induced Pluripotent Mouse Stem Cells by the piggyBac Transposon. *Nat Methods* **6**: 363 – 369.

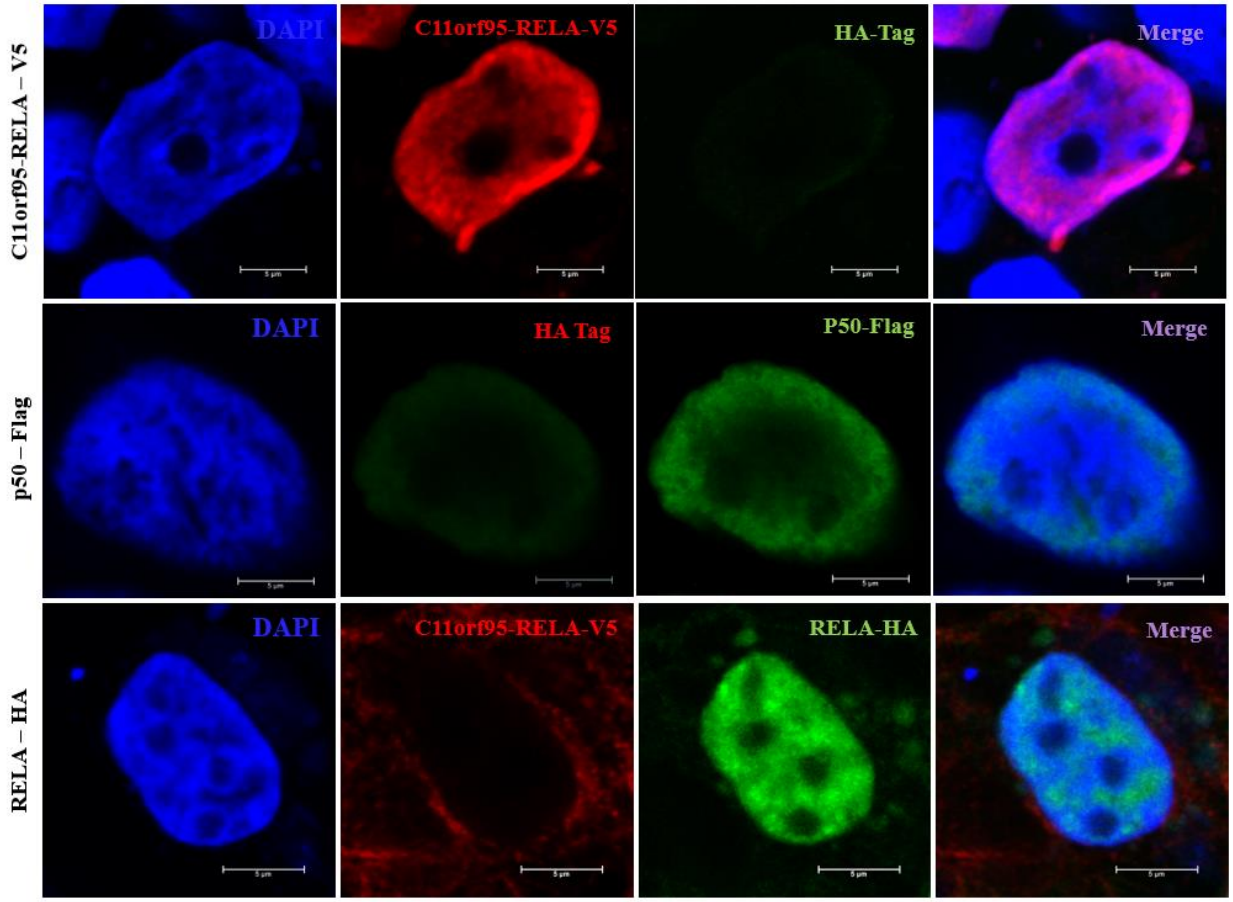

Supplemental Figure 1. The C11orf95-RELA Fusion and NF-κB Subunits p50 and RelA Localize to Nuclei in Hek293T Cells

Scale bar = 5μm.

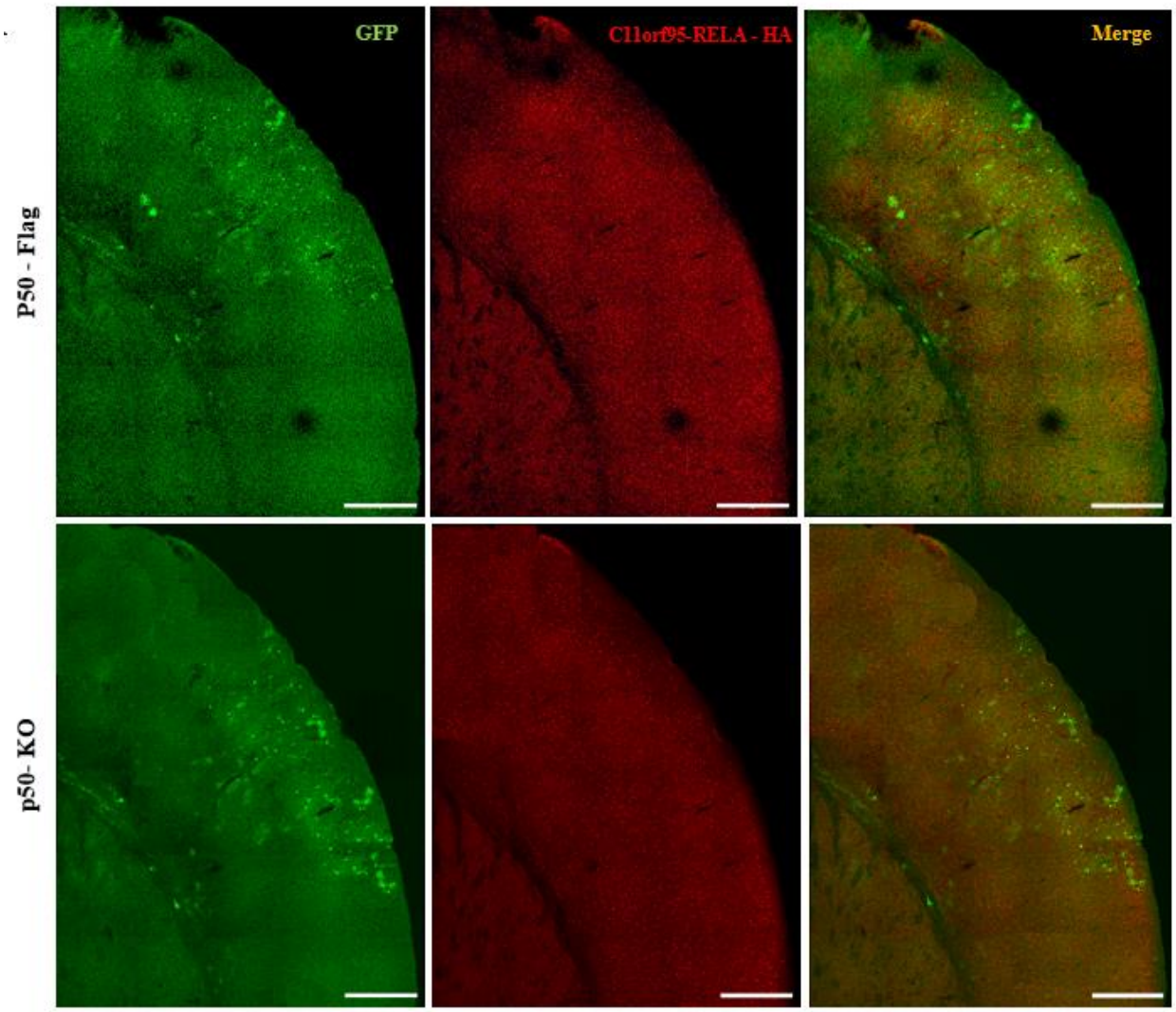

Supplemental Figure 2: Overexpression or Knockdown of p50 Alone does not Generate Tumors

Representative images showing that overexpression or CRISPR/Cas9-mediated knockdown of p50 (without the C11orf95-RELA fusion) is insufficient to generate tumors. Scale bar = 500 µm.

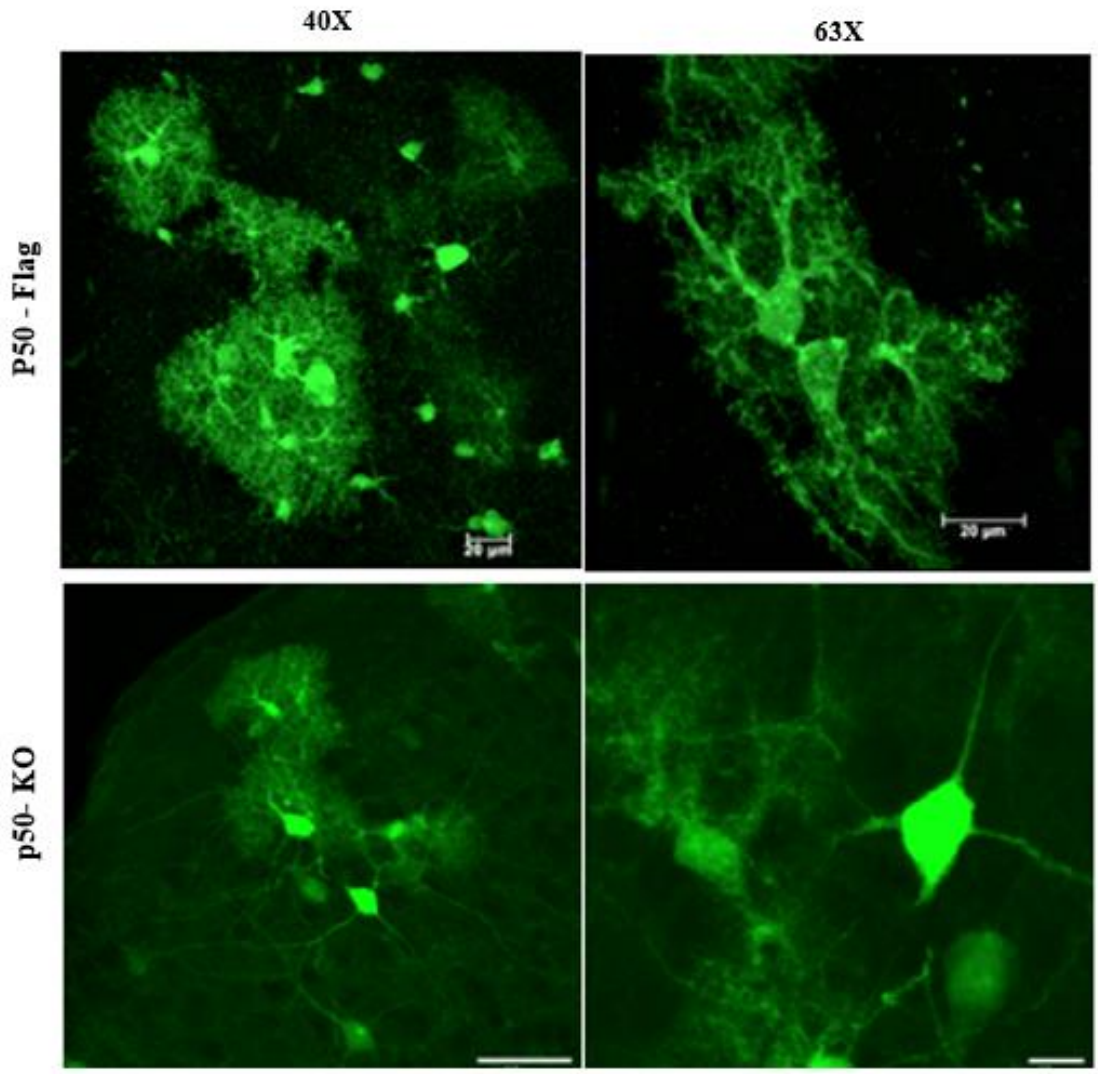

Supplemental Figure 3: Overexpression or Knockdown of p50 Alone does not Generate Altered Transfected Cell Morphology

Representative images showing that overexpression or CRISPR/Cas9-mediated knockdown of p50 (without the C11orf95-RELA fusion) does not generate the aberrant transfected cell morphology seen in C11orf95-RELA + p50-Flag animals. Transfected cells demonstrate normal neuronal and astrocyte morphology.